Deformation of ZrSiO4-MgO aggregates: Deviatoric stress as a control on deformation mechanisms

Xiaoling Zhou [1,2,3,4,*,†] Lianyang Chen,[5,*] Mingzhi Yuan [1,6,*] Feng Lin [2,7] Tian Ye,[5]
Feng Zhao,[8] Martin Kunz,[3] and Lowell Miyagi [2,‡]

[1]*School of Science, Harbin Institute of Technology, Shenzhen, Guangdong 510085, China*
[2]*Department of Geology and Geophysics, University of Utah, Salt Lake City, Utah 84112, USA*
[3]*Advanced Light Source, Lawrence Berkeley National Lab, Berkeley, California 94720, USA*
[4]*Department of Geosciences, Princeton University, Princeton, New Jersey 08542, USA*
[5]*School of Aeronautics, Northwestern Polytechnical University, Xi'an, Shaanxi 710072, China*
[6]*Center for High Pressure Science and Technology Advanced Research, Shanghai 201203, China*
[7]*Department of Aerospace Engineering, Iowa State University, Ames, Iowa 50011, USA*
[8]*Institute for Advanced Study and Institute for Advanced Materials Deformation and Damage from Multi-Scale,
Chengdu University, Chengdu, Sichuan 610106, China*

Deformation behavior of multiphase aggregates has great significance for materials design and understanding the dynamics of the Earth. Here we studied the deformation of zircon (ZrSiO$_4$)-MgO aggregates and found that the introduction of MgO reduced overall deviatoric stress in the aggregates and thus controlled deformation mechanisms of the zircon phase. Zircon primarily deforms by a dominant {101}⟨10−1⟩ slip; however, activity of zircon {100}⟨010⟩ slip increases with the introduction of an increased ratio of MgO into the aggregates, as suggested by the experiments and simulations. We also found both zircon and MgO in the aggregates retained strong deformation texture, which is likely related to the symmetric variants of the dominant slip system of the hard zircon phase. Our results help to clarify the discrepancies in previous studies and understand which phase may dominate the seismic anisotropy in geosciences.

I. INTRODUCTION

Deformation behavior of multiphase aggregates is a fundamental subject for both materials science and Earth sciences. The industrial applications of designed composite materials require the understanding of deformation behavior of multiphase aggregates. In geosciences, it is believed that seismic anisotropy in the Earth's interior is caused by the texture (lattice preferred orientation) of minerals developed during deformation [1–5]. However, most previous deformation studies have focused on single phases [1–5] and there have been fewer studies on multiphase minerals and there is a demand for them. In a few high pressure deformation studies on minerals such as bridgmanite+magnesiowüstite aggregates [6,7] and NaMgF$_3$ perovskite+NaCl aggregates [8], researchers have found that soft phases such as magnesiowüstite and NaCl do not develop texture and the hard phases such as bridgmanite and perovskite develop deformation texture. Instead, deformation on CaGeO$_3$ perovskite+MgO aggregates [9] and NaCl+MgO aggregates [10] indicated that both hard and soft phases developed a texture. It is thus unclear which phase would dominate the texture evolution of the system and whether the phase symmetry has an effect on the texture of the mul-

tiphase. These discrepancies indicate that deformation of multiphase aggregates and the underlying physics warrants further study.

Zircon (ZrSiO$_4$) is a ubiquitous mineral in Earth's crust and a key for geochronology and for recording impact events, but its deformation behavior remains controversial [11–16]. Different dominant slip systems of zircon including {100}⟨010⟩ [11,16], {100}⟨001⟩ [12,13], (001)⟨100⟩ [13,16], and {110}⟨001⟩ [13] have been proposed. A recent diamond anvil cell (DAC) deformation study [17] on zircon-type GdVO$_4$ suggested that GdVO$_4$ deforms by dominant (001)⟨100⟩ and {112}⟨11−1⟩ slip but it remains unclear whether zircon has the same slip activities. Hence an *in situ* deformation study on zircon is expected to resolve the debates on the dominant slip of zircon.

Here we choose pure zircon and zircon-MgO aggregates to study the slip systems of zircon and the deformation behavior of multiphase aggregates at high pressure. Zircon+MgO aggregates represent a combination of tetragonal+cubic symmetries that has not been well explored in previous deformation studies. Additionally, MgO is a common refractory material in industries and the second most abundant material in the Earth's lower mantle [18]. At room temperature MgO deforms primarily by {110}⟨1−10⟩ slip [19]. The good stability of MgO and the relatively simple structures and symmetries of zircon and MgO make them good candidate minerals for this multiphase deformation study. By conducting diamond anvil cell (DAC) combined with synchrotron radial x-ray diffraction (XRD)

---

*These authors contributed equally to this work.

†zhouxiaoling@hit.edu.cn

‡lowell.miyagi@utah.edu

experiments, elastoviscoplastic self-consistent (EVPSC) [20] simulations, and transmission electron microscopy (TEM) characterization, we investigated the deformation slips of zircon and the texture evolution in a single and multiphase system. We show a unique dominant slip of zircon and reveal the correlations between the phase fraction of MgO and deformation mechanisms of zircon. We also discuss how the dominant slip system of one phase influences the texture evolution of another phase in a multiphase system.

II. METHODS

A ground pure zircon powder sample and zircon-MgO mixtures were precompacted and loaded into boron-kapton gaskets mounted in a DAC with 300 μm culet anvils. Pt and MgO were used as pressure calibrants for pure zircon and zircon-MgO mixture deformation experiments, respectively. No pressure medium was used to maximize the differential stress in the chamber. High pressure synchrotron XRD measurements in radial geometry were performed at Beamline 12.2.2 of the Advanced Light Source (ALS), Lawrence Berkeley National Laboratory, USA. A monochromatic beam with energies of 25 and 30 keV was used for the deformation experiments of pure zircon and zircon+MgO mixtures, respectively. The diffraction pattern was refined with the Rietveld method using the Materials Analysis Using Diffraction (MAUD) software [21]. More details could be found in the Supplemental Material [22] (also see [23–26]). The volume ratio of MgO was obtained from the XRD refinements.

The EVPSC code [20] is used to model our experimental data and 12 possible systems including {100}⟨010⟩, {100}⟨001⟩, {100}⟨011⟩, (001)⟨110⟩, (001)⟨100⟩, {101}⟨10−1⟩, {112}⟨11−1⟩, {112}⟨110⟩, {111}⟨1−10⟩, and {110}⟨001⟩ slips, and {112}⟨11−1⟩ twinning and {101}⟨10−1⟩ twinning have been considered in the simulation. Due to the potential effects of the reidite transformation on texture and $Q(hkl)$ evolution we only run simulations for $P < 25$ GPa to minimize the effects of the phase transition. Parameters including the strain, compression rate (strain rate), and critical resolved shear stress (CRSS) values of possible slip systems and twin modes are adjusted to reproduce the experimental lattice strain and texture evolution as a function of pressure. More simulation details can be found in the Supplemental Material [22].

Ground pure zircon and the zircon-MgO mixture powder samples were precompacted and loaded into steel gaskets mounted in a DAC with 300 μm culet anvils. Ruby was used as the pressure calibrant and the highest pressure was increased to ∼30 GPa to minimize the effects of the phase transition. The postdeformed samples were thinned by a focused ion beam (FIB) and prepared for TEM characterization. The energy dispersive spectra (EDS) indicate that the volume ratio of MgO is around 48% in the zircon-MgO mixture. Bright field imaging (BF) and selected area diffraction (SAD) were performed on both the pure sample and the zircon-48% MgO mixture by using a FEI Talos F200X TEM operating at 200 kV. BF and SAD were utilized to examine the dislocation with different slip systems. More analysis can be found in the Supplemental Material [22]; also see [27].

III. RESULTS AND DISCUSSIONS

We observed the zircon ($I4_1/amd$)-reidite ($I4_1/a$) phase transition starting around 20 GPa (Fig. S1 [22]), which was consistent with previous studies [28–30]. Deviatoric lattice strain $Q(hkl)$ and differential/deviatoric stress $t(hkl)$ of each lattice plane of the zircon phase were obtained and calculated. As shown in Fig. 1(a), the (220) planes and (200) planes exhibit the highest and lowest flow strength among the four measured lattice planes in pure zircon. With an increased volume ratio of MgO added to the mixture [Figs. 1(b) and 1(c)], the strength order of the different planes of zircon changes. Specifically, in the 40% MgO sample $t(220)$ of zircon decreases to a similar level as $t(211)$ [Fig. 1(c)]. The overall stress levels decrease significantly compared to stresses in the pure zircon sample which are approximately twice as large as in zircon that is mixed with 40% MgO. The order of $Q(hkl)$ and $t(hkl)$ is directly related to the activity of deformation mechanisms (twinning and dislocations glide). Thus, this change in $t(hkl)$ order and relative magnitude may be related to changes in dislocation or twin activity in the zircon phase.

We analyzed the texture evolution of zircon in the pure and mixed samples during compression [Fig. 1(d)]. As shown by the inverse pole figures (IPFs), in pure zircon a (001) maximum develops at ∼10 GPa and continues to strengthen during further compression [Fig. 1(d)]. In the zircon-25% MgO mixture, zircon first develops a weak (110) maximum that is then overprinted by a (001) texture around ∼13 GPa. In the zircon-40% MgO mixture, zircon initially develops a stronger (110) maximum than the 25% sample, and this is gradually overprinted by a (001) deformation texture. In the 40% MgO sample zircon does not fully develop a (001) texture until ∼38 GPa. Furthermore the texture strength of zircon is considerably lower in the 40% MgO sample than in the pure zircon sample. The fact that the initial (110) texture becomes more pronounced with higher volume fractions of MgO suggests that the addition of a secondary phase has a significant effect on the development of deformation textures in the zircon phase.

The deformation texture change from (110) to (001) suggests a change in the deformation mechanism of zircon. We use the EVPSC method [20] which has been modified for high pressure deformation [31] to simulate the $Q(hkl)$ values and deformation textures of zircon with a range of possible slip and twinning systems including {100}⟨010⟩ [11,16], {100}⟨001⟩ [12,13], (001)⟨100⟩ [13,16], and {110}⟨001⟩ [13] slip systems (see Supplemental Material [22]). We also include slip on {112}⟨11−1⟩ as has been suggested for zircon structured GdVO$_4$ [17] and slip on {101}⟨10−1⟩ which is common in a wide range of tetragonal materials [32–35] and has been proposed for high pressure deformation of stishovite [36]. We tried combinations of these possible slip systems to finely tune the match to experimental textures and $Q(hkl)$ values for pure zircon and zircon mixed with MgO. As shown in Figs. 2(a)–2(c), the simulated $Q(hkl)$ values agree well with the experimental results. The simulated textures reproduce an intense (001) maximum observed in pure zircon and zircon mixed with MgO [Figs. 2(d)–2(f)]. For pure zircon, zircon-25% MgO, and zircon-40% MgO, the simulated maximum texture magnitude is 3.5 multiples of a random distribution
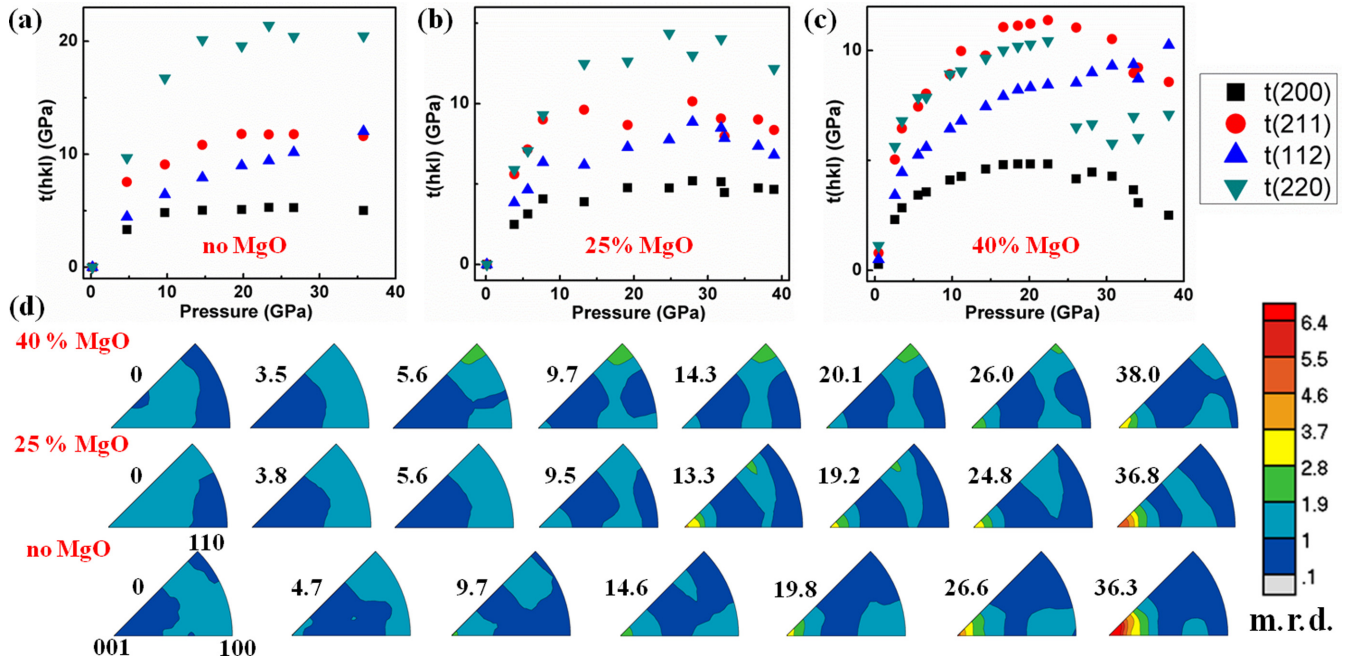
FIG. 1. (a)–(c) Measured mechanical anisotropy change in zircon phase with the introduction of different volume ratios of MgO phase. (d) Measured deformation texture evolution in zircon phase with the introduction of MgO phase at different pressures. The numbers on the left side are pressure in units of GPa.

(m.r.d.) (at a 21% strain, ∼24 GPa), 3.0 m.r.d. (at a 20% strain, ∼25 GPa), and 2.4 m.r.d (at a 17.5% strain, ∼25 GPa), respectively, comparable to the fitted values of 4.4. m.r.d. (at 24 GPa), 3.4 m.r.d. (at 25 GPa), and 2.6 m.r.d (at 26 GPa) ob-

tained from the experiments. We also note that the simulated texture evolution does not fully reproduce the (110) maximum that is observed in the experimental data for the 40% MgO sample and to a lesser extent the 25% MgO sample [Fig. 1(d)].
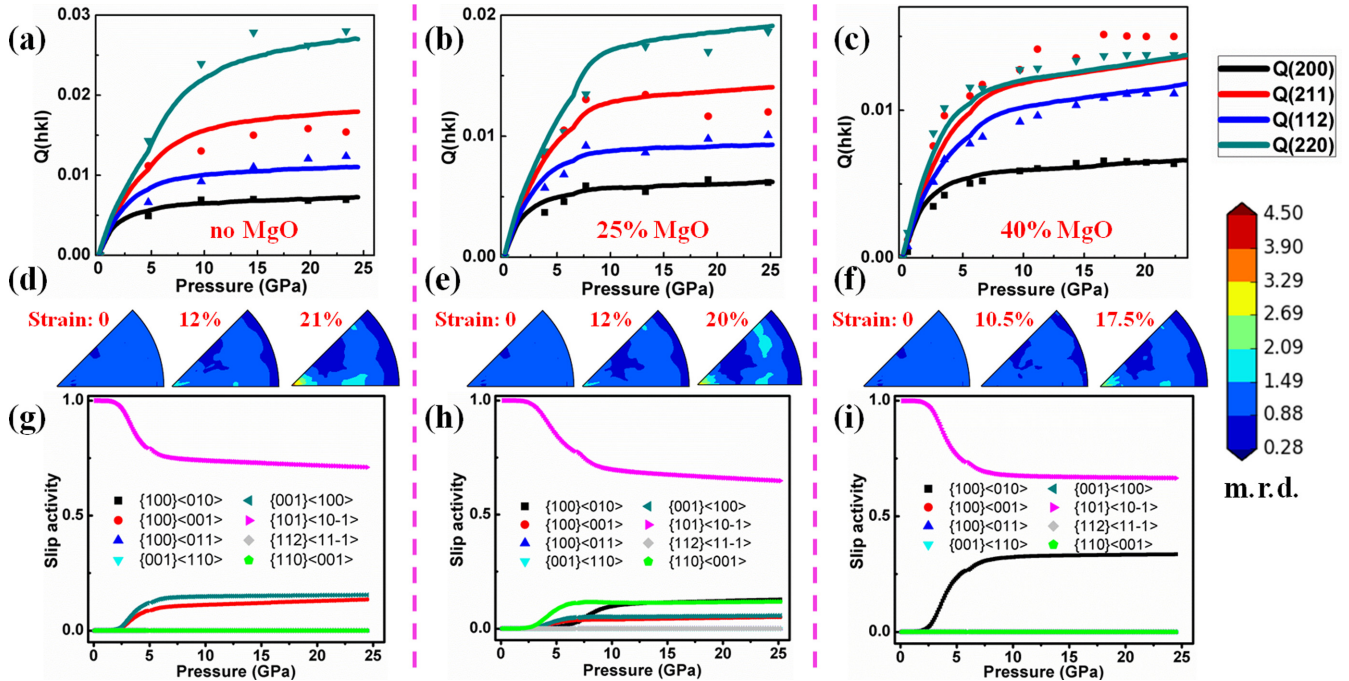

FIG. 2. EVPSC simulation results for $Q(hkl)$ values, texture, and slip activities of the zircon phase: (a), (d), (g) pure zircon, (b), (e), (h) 25% MgO-zircon, and (c), (f), (i) 40% MgO-zircon. The simulated texture is intense in the 001 corner. The maximum texture magnitude is 3.5 m.r.d. for pure zircon at 21% strain (∼24 GPa), 3.0 m.r.d. for zircon mixed with 25% MgO at 20% strain (∼25 GPa), and 2.4 m.r.d. for zircon mixed with 40% MgO at 17.5% strain (∼24 GPa). The parameters used in the EVPSC simulation are listed in Table S1 [22].
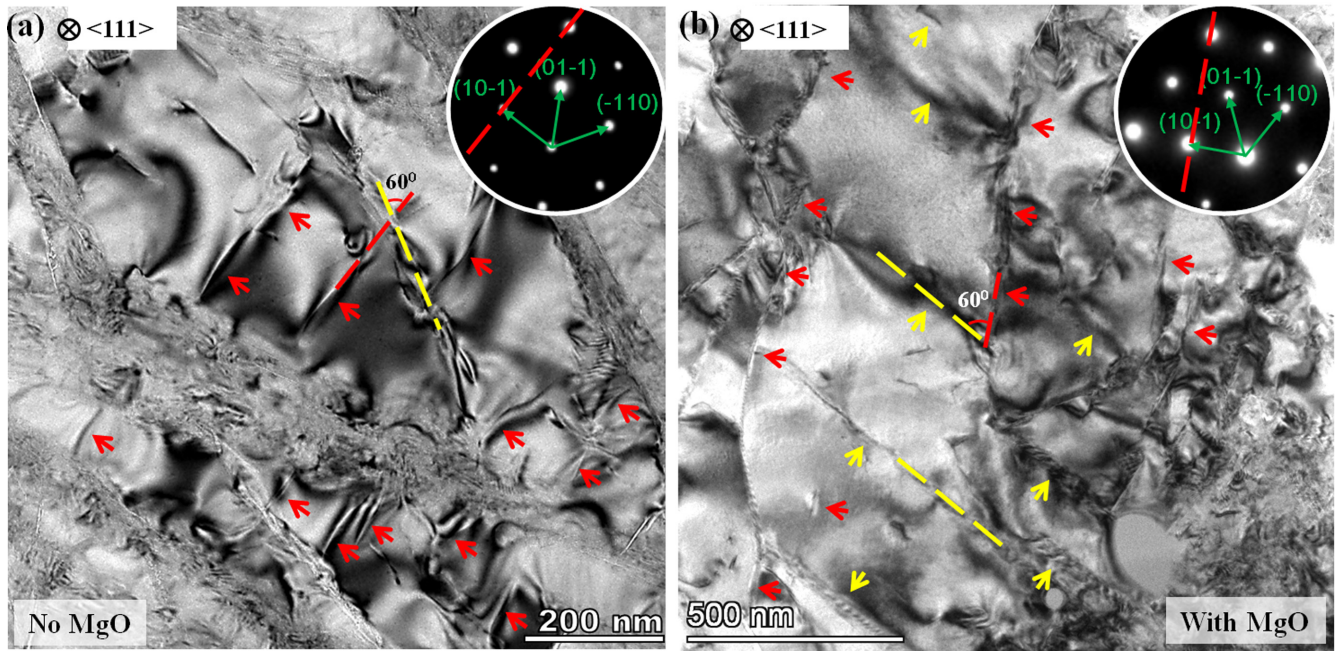
FIG. 3. TEM observations on the microstructures of postdeformed pure sample (a) and the zircon-MgO mixture (b). The insets are the corresponding SAD patterns viewed from the $\langle 111 \rangle$ direction. The red and yellow arrows indicate the $\{101\}\langle 10-1 \rangle$ and $\{100\}\langle 010 \rangle$ dislocations, respectively. The lines are guides for the eyes.

This may be due to the fact that EVPSC and self-consistent simulations in general do not account for the effects of microstructure on texture and lattice strain evolution. Zircon is well known to cleave on $\{110\}$ and it is likely that grinding results in platy grains that are flattened on $\{110\}$. In the 40% MgO sample when zircon grains are fully surrounded by the softer MgO phase, rigid grain rotation may occur resulting in the alignment of zircon grains with $\{110\}$ cleavage planes at high angles to compression. As we do not account for crystallographically flattened grains in our simulations this may be why we fail to reproduce the initial development of a (110) maximum in the experimental IPFs. The EVPSC simulations suggest dominant $\{101\}\langle 10-1 \rangle$ slip to be most consistent with the experimental results [Figs. 2(g)–2(i)]. With the increased volume ratio of MgO, the minor activity of $(001)\langle 100 \rangle$ and $\{100\}\langle 001 \rangle$ slip systems weakens while the activity of $\{100\}\langle 010 \rangle$ slip remarkably increases.

To reveal the physics behind this we performed TEM characterization on the postdeformed samples recovered from high pressure experiments. As shown in Fig. 3(a), high densities of dislocation lines perpendicular to the $\langle 10-1 \rangle$ direction indexed by the SAD pattern were observed in the pure sample, suggesting that the $\{101\}\langle 10-1 \rangle$ slip could be dominant. Remarkably, in the mixed sample another set of dislocations was also found to intersect with the $\{101\}\langle 10-1 \rangle$ slip with an angle of $\sim 60°$ [Fig. 3(b)], which corresponds to the intersection angle between the $\{101\}\langle 10-1 \rangle$ and $\{100\}\langle 010 \rangle$ slips when projected on the (111) plane. Hence, the second set of dislocations was associated with the $\{100\}\langle 010 \rangle$ slip (see Supplemental Material [22] and Fig. S3 therein) and there were increased densities of $\{100\}\langle 010 \rangle$ slips observed in the mixed sample [Fig. 3(b)]. These observations strongly support our results from the EVPSC simulations and XRD experiments that $\{101\}\langle 10-1 \rangle$ is the dominant slip in zircon whereas the

activity of the $\{100\}\langle 010 \rangle$ slip increases with the introduction of MgO into the zircon sample. It is worth noting that deformation bands were also observed in the TEM images, which indicated the severe and heterogeneous deformation of the samples subjected to large shear stress.

The origin of different deformation pathways in zircon should be the deviatoric stress influenced by the introduction of the softer MgO phase. As shown in Figs. 1(a)–1(c), before structural transition (<20 GPa) the average differential/deviatoric stress of zircon gradually decreases with the increase of MgO and $t(220)$ becomes comparable to $t(211)$ in zircon mixed with 40% of MgO. This suggests that the overall shear stress imposed on zircon decreases and the stress field in zircon redistributes because of the introduction of the softer MgO phase. The change in stress field may result in the modification of atomic densities in crystallographic planes. Generally the crystallographic plane with a larger d spacing exhibits a higher atomic density and is more energetically favorable when the slip occurs. In this case the d spacing of the (100) plane is larger than the (101) plane (Fig. S4 [22]), indicating that the slip on the (100) plane is more energetically favorable at low deviatoric stress. Meanwhile, the differences in d spacing between the (100) and (101) planes are systematically larger in zircon mixed with MgO than that of the pure sample (Fig. S4 [22]), suggesting that the atomic density of the (100) plane is relatively increased comparing to the (101) plane and thus the (100) slip is more favorable in the mixed sample than that in the pure sample.

Interestingly dislocations with $\langle 10-1 \rangle$ Burgers vectors are found in our experiments though it is not energetically favorable. Slip on $\{101\}\langle 10-1 \rangle$ is common in tetragonal ceramics [32–35] and is suggested for high pressure deformation of stishovite [36]. High deviatoric stress levels and low temper-
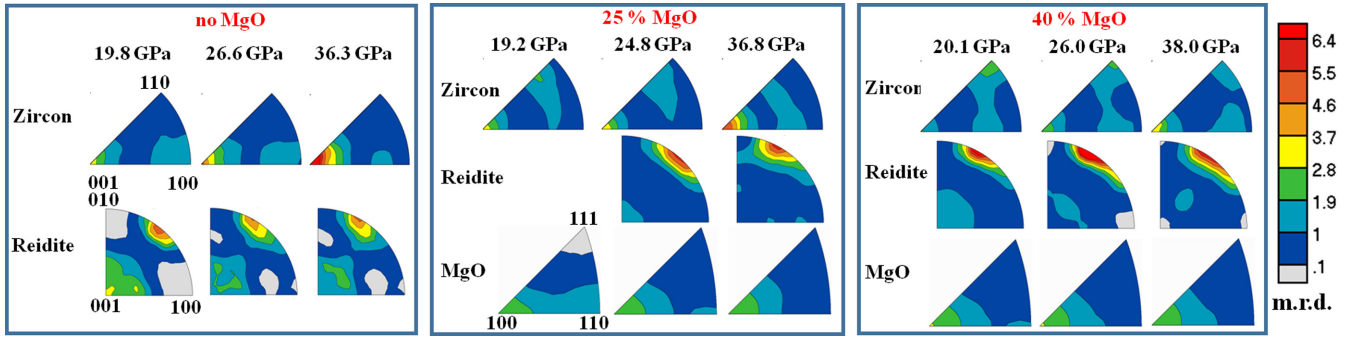
FIG. 4. Texture evolutions of zircon, reidite, and MgO with increased pressure. The IPFs of the reidite phase are asymmetric so that a sector of 90° is used.

atures in our experiments appear to favor activation of the {101}⟨10−1⟩ slip system in zircon. The high deviatoric stress in our experiments causes dominant {101}⟨10−1⟩ slip while the introduction of softer MgO reduces the shear stress on zircon and allows the activation of the {100}⟨010⟩ system which is generally energetically favorable at low deviatoric stress. In a TEM study on natural zircon samples [37], higher stress conditions tended to result in activation of higher order slip systems, while in contrast zircon grains contained in a softer matrix tended to only deform by energetically favorable slip systems such as {100}⟨010⟩. This is consistent with our results that the {100}⟨010⟩ slip system is energetically favorable at low deviatoric stress and the deviatoric stress controls the deformation mechanisms of zircon.

Our analysis shows distinct results from previous experimental studies on slip systems of zircon. In natural zircon samples, compositional variation or chemical environment change might be the cause for different slip system activities. Zircon deformed by tectonic events or shock compression experiences distinctly different strain rate and high temperature processing comparing with static DAC compression. Studies on olivine suggested that factors such as strain rate, temperature, pressure, deviatoric stress, and chemical conditions including water and oxygen fugacity, would play roles in changing the slip system and texture type of olivine [1,4,38]. In this scenario, either change in composition or chemical environment in natural samples or change in strain rate and temperature in previous tectonic events or shock experiments could lead to different slip systems of zircon. Our DAC experiments suggest a dominant {101}⟨10−1⟩ slip system in zircon, and provide evidence that the deviatoric stress variation controlled by physically tuning phase fraction of aggregates could result in different slip activities of zircon. This helps to understand the discrepancies in deformation mechanisms of natural zircon samples or zircon deformed by tectonic events, shock compression, and DAC. It can also explain differences in slip activities and deformation behavior of the same phase in a single and multiphase system. Since the Earth's rocks are natural multiphase systems, deformation experiments and modeling on multiphase system should take the place of single minerals in the future.

We also compared the texture evolution of reidite and MgO in the pure sample and mixed samples across the phase transition (Fig. 4). Reidite in both pure phase and mixtures shows a strong (110) transformation texture inherited from the

(001) maxima in zircon. It can be seen that MgO mixed with 75% zircon and 60% zircon both develop a (100) deformation texture (Fig. 4). This is in contrast to previous studies in which the soft magnesiowüstite and NaCl phases remain random [6,8]. Our result is more similar to the texture evolution in the CaGeO₃ + MgO and NaCl+MgO deformation studies where both phases develop texture [9,10].

Previous studies documenting texture disruption in the soft phase either contain hard phases that remain undeformed [39–41] or hard phases with low symmetry and a dominant slip system with few or no symmetric variants [7,8]. Numerical simulations and microstructure observations show heterogeneous strain fields within the soft phase which results in a lack of texture development [8,39]. In our case, zircon has the highest differential stress (Fig. S1 [22]) and is much harder than MgO. We summarized the dominant slips and their symmetric variants of hard phases from previous studies in Table I. It is likely that when the hard phase has a dominant slip with few symmetric variants, it imposes more strain heterogeneity and tends to disrupt the texture in the soft phase. Instead a hard phase with dominant slip systems that have many symmetric variants does not impose much strain heterogeneity in the soft phase so the texture of the soft phase is preserved. In our study, zircon has a dominant {101}⟨10−1⟩ slip system with four symmetric variants, which might be the reason for the preservation of texture in the soft MgO phase. This is also supported by previous studies [9,10] in which both CaGeO₃ and MgO have dominant slips with six symmetric variants and the soft phase develops texture. Further studies are required to confirm this hypothesis. Our results show the correlations between slip system and texture evolution of hard and soft phases in multiphase systems. It helps to understand texture evolution of minerals in multiphase system and determine the phase accounting for the seismic anisotropy.

IV. CONCLUSIONS

In summary, our study suggests that the introduction of MgO decreases the deviatoric stress in zircon and controls its deformation mechanisms. EVPSC simulations and TEM characterization indicate that zircon deforms by a dominant {101}⟨10−1⟩ slip but the activity of zircon {100}⟨010⟩ slip increases with the introduction of an increased ratio of MgO, suggesting stress-sensitive deformation pathways of zircon

TABLE I. The correlations between dominant slip of the hard phase and the texture evolution of the soft phase. Phase fraction of the soft phase is below 50%.

Hard phase (+ soft phase)	Dominant slip of hard phase	Symmetric variants	Soft phase	Reference
$CaGeO_3$(+MgO)	$\{110\}\langle1-10\rangle$	6	Texture	Ref. [9]
MgO (+NaCl)	$\{110\}\langle1-10\rangle$	6	Texture	Ref. [10]
Zircon (+MgO)	$\{101\}\langle10-1\rangle$	4	Texture	This study
$(Mg, Fe)SiO_3$ (bridgmanite) [+(Mg,Fe)O]	(100)[010]	1	No texture	Ref. [7]
$NaMgF_3$ (perovskite) (+NaCl)	(100)[010]	1	No texture	Ref. [8]

controlled by the second phase. We also found that the MgO phase in the aggregates develops a strong (100) deformation texture in contrast to previous studies on orthorhombic+cubic aggregates in which the MgO phase tends to have a random orientation distribution. This is likely related to the symmetric variants of the dominant slip system of the hard phase and the degree of strain heterogeneity that the hard phase imposes in the softer phase. Our results provide insight into understanding the role of deviatoric stress levels in controlling zircon deformation pathways, especially in understanding the discrepancies in previous deformation studies. It also implies that through the introduction of a secondary phase one can adjust the deviatoric stress and control the deformation mechanisms of targeted materials.

[1] H. Jung and S.-I. Karato, Science **293**, 1460 (2001).

[2] S. Merkel, A. Kubo, L. Miyagi, S. Speziale, T. S. Duffy, H. K. Mao, and H. R. Wenk, Science **311**, 644 (2006).

[3] S. Merkel, A. K. McNamara, A. Kubo, S. Speziale, L. Miyagi, Y. Meng, T. S. Duffy, and H. R. Wenk, Science **316**, 1729 (2007).

[4] H. Jung, W. Mo, and H. W. Green, Nat. Geosci. **2**, 73 (2008).

[5] L. Miyagi, W. Kanitpanyacharoen, P. Kaercher, K. K. Lee, and H. R. Wenk, Science **329**, 1639 (2010).

[6] J. Girard, G. Amulele, R. Farla, A. Mohiuddin, and S.-I. Karato, Science **351**, 144 (2016).

[7] L. Miyagi and H.-R. Wenk, Phys. Chem. Miner. **43**, 597 (2016).

[8] P. Kaercher, L. Miyagi, W. Kanitpanyacharoen, E. Zepeda-Alarcon, Y. Wang, D. Parkinson, R. Lebensohn, F. De Carlo, and H. Wenk, Earth Planet. Sci. Lett. **456**, 134 (2016).

[9] Y. Wang, N. Hilairet, N. Nishiyama, N. Yahata, T. Tsuchiya, G. Morard, and G. Fiquet, Geochem. Geophys. Geosyst. **14**, 3389 (2013).

[10] F. Lin, M. Giannetta, M. Jugle, S. Couper, B. Dunleavy, and L. Miyagi, Minerals **9**, 679 (2019).

[11] H. Leroux, W. Reimold, C. Koeberl, U. Hornemann, and J.-C. Doukhan, Earth Planet. Sci. Lett. **169**, 291 (1999).

[12] S. M. Reddy, N. E. Timms, W. Pantleon, and P. Trimby, Contrib. Mineral. Petrol. **153**, 625 (2007).

[13] M.-A. Kaczmarek, S. Reddy, and N. E. Timms, Lithos **127**, 414 (2011).

[14] D. Moser, C. Cupelli, I. Barker, R. Flowers, J. Bowman, J. Wooden, and J. Hart, Can. J. Earth Sci. **48**, 117 (2011).

[15] I. Morozova, S. R. Shieh, D. E. Moser, I. R. Barker, and J. M. Hanchar, in *Microstructural Geochronology: Planetary Records Down to Atom Scale*, edited by D. E. Moser, F. Corfu, J. R. Darling, S. M. Reddy, and K. Tait (Wiley, New York, 2018), p. 167.

[16] N. E. Timms, D. Healy, T. M. Erickson, A. A. Nemchin, M. A. Pearce, and A. J. Cavosie, in *Microstructural Geochronology: Planetary Records Down to Atom Scale*, edited by D. E. Moser, F. Corfu, J. R. Darling, S. M. Reddy, and K. Tait (Wiley, New York, 2018), p. 183.

[17] B. Yue, F. Hong, S. Merkel, D. Tan, J. Yan, B. Chen, and H.-K. Mao, Phys. Rev. Lett. **117**, 135701 (2016).

[18] X. Li, Y. Yuan, J. Zhang, T. Kim, D. Zhang, K. Yang, Y. Lee, and L. Wang, J. Phys.: Condens. Matter **30**, 194002 (2018).

[19] S. Merkel, H. R. Wenk, J. Shu, G. Shen, P. Gillet, H.-k. Mao, and R. J. Hemley, J. Geophys. Res.: Solid Earth **107**, ECV 3-1 (2002).

[20] H. Wang, P. Wu, C. Tomé, and Y. Huang, J. Mech. Phys. Solids **58**, 594 (2010).

[21] L. Lutterotti, R. Vasin, and H.-R. Wenk, Powder Diffr. **29**, 76 (2014).

[22] See Supplemental Material at http://link.aps.org/supplemental/10.1103/PhysRevB.105.L220101 for methods and supplemental figures and table.

[23] A. K. Singh, C. Balasingh, H.-k. Mao, R. J. Hemley, and J. Shu, J. Appl. Phys. **83**, 7567 (1998).

[24] H. Özkan and J. Jamieson, Phys. Chem. Miner. **2**, 215 (1978).

[25] R. Dutta and N. Mandal, Mater. Chem. Phys. **135**, 322 (2012).

[26] H.-R. Wenk, L. Lutterotti, P. Kaercher, W. Kanitpanyacharoen, L. Miyagi, and R. Vasin, Powder Diffr. **29**, 220 (2014).

[27] C. Y. Wang, C. M. Cepeda-Jiménez, and M. T. Pérez-Prado, Acta Mater. **194**, 190 (2020).

[28] R. M. Hazen and L. W. Finger, Am. Mineral. **64**, 196 (1979).

[29] M. Marqués, J. Contreras-García, M. Florez, and J. Recio, J. Phys. Chem. Solids **69**, 2277 (2008).

[30] K. Kusaba, T. Yagi, M. Kikuchi, and Y. Syono, J. Phys. Chem. Solids **47**, 675 (1986).

[31] F. Lin, N. Hilairet, P. Raterron, A. Addad, J. Immoor, H. Marquardt, C. Tomé, L. Miyagi, and S. Merkel, J. Appl. Phys. **122**, 205902 (2017).

[32] M. Leoni, J. Martinez-Garcia, and P. Scardi, J. Appl. Crystallogr. **40**, 719 (2007).

[33] X. Tan and J. K. Shang, J. Phys.: Condens. Matter **16**, 1455 (2004).

[34] M. Blanchin, L. Bursill, and C. Lafage, Proc. R. Soc. London, Ser. A **429**, 175 (1990).

[35] K. Ashbee and R. Smallman, J. Am. Ceram. Soc. **46**, 211 (1963).

[36] P. M. Kaercher, E. Zepeda-Alarcon, V. B. Prakapenka, W. Kanitpanyacharoen, J. S. Smith, S. Sinogeikin, and H.-R. Wenk, Phys. Chem. Miner. **42**, 275 (2015).

[37] E. Kovaleva, U. Klötzli, G. Habler, and J. Wheeler, Am. Mineral. **100**, 1834 (2015).

[38] S.-i. Karato, H. Jung, I. Katayama, and P. Skemer, Annu. Rev. Earth Planet. Sci. **36**, 59 (2008).

[39] G. Canova, H. Wenk, and A. Molinari, Acta Metall. Mater. **40**, 1519 (1992).

[40] A. Poudens, B. Bacroix, and T. Bretheau, Mater Sci. Eng.: A **196**, 219 (1995).

[41] G. Garcés, M. Rodríguez, P. Perez, and P. Adeva, Mater Sci. Eng.: A **419**, 357 (2006).